 CMC, vol.23, no.2, pp.155-185, 2011

The Global Nonlinear Galerkin Method for the Solution of von Karman Nonlinear Plate Equations: An Optimal & Faster Iterative Method for the Direct Solution of Nonlinear Algebraic Equations $\mathbf{F}(\mathbf{x}) = \mathbf{0}$, using $\dot{\mathbf{x}} = \lambda[\alpha\mathbf{F} + (1-\alpha)\mathbf{B}^{\mathbf{T}}\mathbf{F}]$

Hong-Hua Dai[1,2], Jeom Kee Paik[3] and S. N. Atluri[2]

Abstract: The application of the Galerkin method, using global trial functions which satisfy the boundary conditions, to nonlinear partial differential equations such as those in the von Karman nonlinear plate theory, is well-known. Such an approach using trial function expansions involving multiple basis functions, leads to a highly coupled system of nonlinear algebraic equations (NAEs). The derivation of such a system of NAEs and their direct solutions have hitherto been considered to be formidable tasks. Thus, research in the last 40 years has been focused mainly on the use of local trial functions and the Galerkin method, applied to the piecewise linear system of partial differential equations in the updated or total Lagrangean reference frames. This leads to the so-called tangent-stiffness finite element method. The piecewise linear tangent-stiffness finite element equations are usually solved by an iterative Newton-Raphson method, which involves the inversion of the tangent-stiffness matrix during each iteration. However, the advent of symbolic computation has made it now much easier to directly derive the coupled system of NAEs using the global Galerkin method. Also, methods to directly solve the NAEs, without inverting the tangent-stiffness matrix during each iteration, and which are faster and better than the Newton method are slowly emerging. In a previous paper [Dai, Paik and Atluri (2011a)], we have presented an exponentially convergent scalar homotopy algorithm to directly solve a large set of NAEs arising out of the application of the global Galerkin method to von Karman plate equations. While the results were highly encouraging, the computation time increases with the increase in the number of NAEs—the number of coupled NAEs solved by Dai, Paik and Atluri (2011a) was of the order of 40. In this paper we present a much improved

[1] College of Astronautics, Northwestern Polytechnical University, Xi'an 710072, P.R. China
[2] Center for Aerospace Research & Education, University of California, Irvine
[3] Lloyd's Register Educational Trust (LRET) Center of Excellence, Pusan National University, Korea

method of solving a larger system of NAEs, much faster. If $\mathbf{F}(\mathbf{x}) = 0$ $[F_i(x_j) = 0]$ is the system of NAEs governing the modal amplitudes x_j $[j = 1,\ 2...N]$, for large N, we recast the NAEs into a system of nonlinear ODEs: $\dot{\mathbf{x}} = \lambda[\alpha\mathbf{F} + (1-\alpha)\,\mathbf{B}^{\mathrm{T}}\mathbf{F}]$, where λ and α are scalars, and $B_{ij} = \partial F_i/\partial x_j$. We derive a purely iterative algorithm from this, with optimum value for λ and α being determined by keeping $\mathbf{x}$ on a newly defined invariant manifold [Liu and Atluri (2011b)]. Several numerical examples of nonlinear von Karman plates, including the post-buckling behavior of plates with initial imperfections are presented to show that the present algorithms for directly solving the NAEs are several orders of magnitude faster than those in Dai, Paik and Atluri (2011a). This makes the resurgence of simple global Galerkin methods, as alternatives to the finite element method, to directly solve nonlinear structural mechanics problems without piecewise linear formulations, entirely feasible.

Keywords: large deflections, global nonlinear Galerkin method, von Karman plate equations, nonlinear algebraic equations (NAEs), initial guess, optimal vector-driven algorithm (OVDA), new manifold

1 Introduction

Ingenious ways of using von Karman's nonlinear theory for moderate rotations, in an updated Lagrangian corotational frame, for analyzing large rotations, and large deformation of plates and shells, have been proposed by Cai, Paik and Atluri (2009a, 2009b, 2010a, 2010b) and Zhu, Cai, Paik and Atluri (2010). In von Karman's theory, the large deflection behavior of plates with initial imperfections is described by two nonlinear PDEs which are notoriously difficult to solve. In general, the exact analytical solution of PDEs are possible only in the simplest geometrical domains, and only mostly for linear problems [Atluri 2002]. Therefore, for solving the von Karman PDEs, researchers turn to the numerical methods.

For nonlinear problems, such as the von Karman nonlinear theory of plates, it is these days very common to develop the tangent-stiffness finite element method, based on local trial function in each element, using the incremental form of the symmetric Galerkin weak-form. The tangent-stiffness equations of the nonlinear plate theory are solved by using Newton-Raphson iteration scheme for each incremental displacement state, which is only quadratically convergent. Moreover, the Newton method involves the expensive process of inverting the tangent-stiffness at each iteration.

To avoid the expensive effort due to solving such a large set of equations as in the finite element method, an incremental global Galerkin method was first proposed by Ueda, Rashed and Paik (1987), and applied by Paik, Thayamballi, Lee and

Kang (2001), Paik and Lee (2005). In the incremental global Galerkin method, instead of solving the von Karman PDEs directly, an incremental form of governing differential equations is derived. The derived PDEs are a set of piecewise linear partial differential equations. Therefore, upon applying the global Galerkin method to the incremental form of governing differential equations, a set of linear system of simultaneous equations will be obtained. This incremental global Galerkin method naturally leads to a tangent-stiffness matrix which is in general densely populated [as opposed to the sparsely populated tangent-stiffness matrix of the plates, based on the finite element method], but the matrix is of a much smaller size than that in FEM. However, the solution of the nonlinear plate problem, using the incremental global Galerkin method of Ueda, Rashed and Paik (1987) also involves a Newton-Raphson iteration, and the inversion of the tangent-stiffness matrix at each time and is only quadratically convergent.

Unlike the above methods, in the present paper the global Galerkin method is applied directly to the von Karman equations to derive a system of third order coupled NAEs. As a contribution of this study, we solve the resultant large set of NAEs directly in each load step by introducing a highly efficient algorithm which does not involve the inversion of the Jacobian tangent-stiffness matrix. In general, the resultant NAEs is hard to solve. Firstly, one has to find the one physical solution among the multiple solutions. Therefore, a suitable initial guess is required to lead to the real solution. To keep track of the physical solution, we will solve the sets of NAEs corresponding to gradually increased loads, and take the solution of the last load step as the initial guess for the current NAEs under the current loads. Secondly, the size of NAEs grows large dramatically, with the increase of the number of terms of the deflection function. However, there are few tools to solve such a large system of NAEs directly. The most well-known Newton method suffers from its sensitivity to initial guess and being very expensive for calculating the inverse of the Jacobian matrix at each iteration step. Because of these two reasons, solving the von Karman equations by the global nonlinear Galerkin method is thought to be an impossible task until the work by Dai, Paik and Atluri (2011a), where they use the exponentially convergent scalar homotopy algorithm (ECSHA) to solve the large set of NAEs. Recently, six algorithms are developed to directly deal with the NAEs without calculating the inverse of the Jacobian matrix. They are the fictitious time integration method (FTIM) [Liu and Atluri (2008)], the modified Newton method [Atluri, Liu and Kuo (2009)], the scalar homotopy method (SHM) [Liu, Yeih, Kuo and Atluri (2009)], the exponentially convergent scalar homotopy algorithm [Liu, Ku, Yeih, Fan and Atluri (2010)], a residual-norm based iterative algorithm [Liu and Atluri (2011a)] and the optimal vector-driven algorithm (OVDA) [Liu and Atluri (2011b)]. Of these, the iterative OVDA algorithm [Liu and Atluri

(2011b)] promises to be the best, and much faster than the Newton method. In this iterative method, the system of nonlinear equations $\mathbf{F}(\mathbf{x})=0$ $[F_i(x_j)=0]$ governing the global Galerkin modal amplitudes x_j are solved by first converting the NAEs into a system of nonlinear ODEs: $\dot{\mathbf{x}}=\lambda[\alpha\mathbf{F}+(1-\alpha)\mathbf{B}^{\mathrm{T}}\mathbf{F}]$, where λ and α are scalars, and $B_{ij}=\partial F_i/\partial x_j$. We derive a purely iterative algorithm from this, with optimum values for λ and α being determined to keep $\mathbf{x}$ on a newly defined manifold. The present OVDA algorithm is several orders of magnitude faster than either the ECSHA used in Dai, Paik and Atluri (2011a) or the Newton algorithm. Several numerical examples of nonlinear von Karman plates, including post-buckling behavior of plates with initial imperfections, are presented to show that the present algorithms for directly solving the NAEs are several orders of magnitude faster than those in Dai, Paik and Atluri (2011a). The ideas presented in this paper and the state of the science in symbolic computation, make the resurgence of the global Galerkin method, as an efficient and simple tool to quickly solve nonlinear structural mechanics problems, possible.

2 Governing differential equations of plates and the global nonlinear Galerkin method

The elastic large deflection response of a plate with initial imperfection is governed by two PDEs, which are named von Karman plate equations. One of them represents the equilibrium condition in the transverse direction, and the other represents the compatibility condition of in-plane strains. The PDEs are as follows:

$$\varphi = D\nabla^4 w - t\left[\frac{\partial^2 F}{\partial y^2}\frac{\partial^2(w+w_0)}{\partial x^2}+\frac{\partial^2 F}{\partial x^2}\frac{\partial^2(w+w_0)}{\partial y^2}-2\frac{\partial^2 F}{\partial x\partial y}\frac{\partial^2(w+w_0)}{\partial x\partial y}\right]-Q = 0 \tag{1}$$

$$\nabla^4 F = E\left[\left(\frac{\partial^2 w}{\partial x\partial y}\right)^2-\frac{\partial^2 w}{\partial x^2}\frac{\partial^2 w}{\partial y^2}+2\frac{\partial^2 w_0}{\partial x\partial y}\frac{\partial^2 w}{\partial x\partial y}-\frac{\partial^2 w_0}{\partial x^2}\frac{\partial^2 w}{\partial y^2}-\frac{\partial^2 w}{\partial x^2}\frac{\partial^2 w_0}{\partial y^2}\right] \tag{2}$$

In the above, w_0 is the given initial transverse displacement, w is the additional transverse displacement, and F is the Airy stress function governing the in plane stress resultants. In solving the above PDEs by the direct nonlinear global Galerkin method for capturing elastic large deflections of a simply supported plate, the added deflection w due to the applied load, and the initial deflection w_0 should satisfy the boundary conditions at four edges. In particular, the boundary conditions are as

Table 1: Notations

a	length of the plate
b	width of the plate
t	thickness of the plate
α	aspect ratio a/b
E	Young's modulus
υ	Poisson's ratio
$D = \frac{Et^3}{12(1-\upsilon^2)}$	plate bending rigidity
w	added deflection of the plate
w_0	initial deflection of the plate
F	Airy stress function
M	assumed half wave number in the x direction
N	assumed half wave number in the y direction
P_x	compression force in the x direction
P_y	compression force in the y direction
M_x	in-plane bending moment in the x direction
M_y	in-plane bending moment in the y direction
τ	shear stress
Q	lateral pressure
σ_{rx}	residual stress in the x direction
σ_{ry}	residual stress in the y direction

follows:

$$\begin{aligned} &w = 0, \quad \frac{\partial^2 w}{\partial y^2} + \upsilon \frac{\partial^2 w}{\partial x^2} = 0, \ \textit{at } y = 0, \textit{ and } y = b \\ &w = 0, \quad \frac{\partial^2 w}{\partial x^2} + \upsilon \frac{\partial^2 w}{\partial y^2} = 0, \ \textit{at } x = 0, \textit{ and } x = a \end{aligned} \tag{3}$$

To satisfy the boundary conditions, the added deflection function w and the initial deflection w_0 can be assumed in Fourier series,

$$w_0 = \sum_{m=1}^{M} \sum_{n=1}^{N} A_{0mn} \sin(\frac{m\pi x}{a}) \sin(\frac{n\pi y}{b}) \tag{4}$$

$$w = \sum_{m=1}^{M}\sum_{n=1}^{N} A_{mn}\sin(\frac{m\pi x}{a})\sin(\frac{n\pi y}{b}) \tag{5}$$

Where, A_{mn} and A_{0mn} are the unknown and the known coefficients, respectively. The conditions of the combined loads, namely, bi-axial loads, bi-axial in-plane bending and edge shear are given as follows:

$$\begin{aligned}
&\int_0^b \frac{\partial^2 F}{\partial y^2} t\,dy = P_x, \quad \int_0^b \frac{\partial^2 F}{\partial y^2} t(y-\frac{b}{2})dy = M_x \ \ at\ x=0,\ and\ x=a \\
&\int_0^a \frac{\partial^2 F}{\partial x^2} t\,dx = P_y, \quad \int_0^a \frac{\partial^2 F}{\partial x^2} t(x-\frac{a}{2})dx = M_y \ \ at\ y=0,\ and\ x=b \\
&\frac{\partial^2 F}{\partial x \partial y} = -\tau, \ \ at\ four\ edges
\end{aligned} \tag{6}$$

Then the homogenous solution F_h for the Airy stress function F should satisfy the condition of the combined loads acting on the plate. Considering the loading conditions, we can easily find F_h , by assuming F_h as cube polynomials in x and y. Substituting F_h into Eq. (6) we can obtain,

$$F_h = -P_x\frac{y^2}{2bt} - \sigma_{rx}\frac{y^2}{2} - P_y\frac{x^2}{2at} - \sigma_{ry}\frac{x^2}{2} - M_x\frac{y^2(2y-3b)}{b^3 t} - M_y\frac{x^2(2x-3a)}{a^3 t} - \tau_{xy}xy \tag{7}$$

For simplicity, the following notations are introduced to abbreviate the expressions involving the sine or cosine terms,

$$\begin{aligned}
&\sin(\frac{m\pi x}{a}) = sx(m), \quad \cos(\frac{m\pi x}{a}) = cx(m) \\
&\sin(\frac{n\pi y}{b}) = \ \ sy(n), \quad \cos(\frac{n\pi y}{b}) = cy(n)
\end{aligned} \tag{8}$$

To find the particular solution F_{p}, which should satisfy Eq. (2) , one can substitute w and w_0 into the right side of Eq. (2), thus obtaining:

$$\begin{aligned}
&\nabla^4 F_p = \frac{E\pi^4}{4a^2b^2} \\
&\sum_{m=1}^{M}\sum_{n=1}^{N}\sum_{k=1}^{K}\sum_{l=1}^{L}\big\{[A_{mn}A_{kl}ml(nk-ml) - A_{kl}A_{0mn}(nk-ml)^2]cx(m+k)cy(n+l) \\
&+[A_{mn}A_{kl}ml(nk+ml) + A_{kl}A_{0mn}(nk+ml)^2]cx(m+k)cy(n-l) \\
&+[A_{mn}A_{kl}ml(nk+ml) + A_{kl}A_{0mn}(nk+ml)^2]cx(m-k)cy(n+l) \\
&+[A_{mn}A_{kl}ml(nk-ml) - A_{kl}A_{0mn}(nk-ml)^2]cx(m-k)cy(n-l)\big\}
\end{aligned} \tag{9}$$

Consequently, the particular solution F_p for the Airy stress function can be written in the following way,

$$\begin{aligned} F_p = \sum_{m=1}^{M}\sum_{n=1}^{N}\sum_{k=1}^{K}\sum_{l=1}^{L}\{\ & B_1(m,n,k,l)\times cx(m+k)cy(n+l) \\ & + B_2(m,n,k,l)\times cx(m+k)cy(n-l) \\ & + B_3(m,n,k,l)\times cx(m-k)cy(n+l) \\ & + B_4(m,n,k,l)\times cx(m-k)cy(n-l)\} \end{aligned} \tag{10}$$

Upon substituting F_p into the Eq. (2), the coefficients B_1, B_2, B_3 and B_4 are obtained as

$$\begin{aligned} B_1(m,n,k,l) &= \frac{E\alpha^2}{4}\times\frac{A_{mn}A_{kl}ml(nk-ml)-A_{kl}A_{0mn}(nk-ml)^2}{[(m+k)^2+(n+l)^2]^2} \\ B_2(m,n,k,l) &= \frac{E\alpha^2}{4}\times\frac{A_{mn}A_{kl}ml(nk+ml)+A_{kl}A_{0mn}(nk+ml)^2}{[(m+k)^2+(n-l)^2]^2} \\ B_3(m,n,k,l) &= \frac{E\alpha^2}{4}\times\frac{A_{mn}A_{kl}ml(nk+ml)+A_{kl}A_{0mn}(nk+ml)^2}{[(m-k)^2+(n+l)^2]^2} \\ B_4(m,n,k,l) &= \frac{E\alpha^2}{4}\times\frac{A_{mn}A_{kl}ml(nk-ml)-A_{kl}A_{0mn}(nk-ml)^2}{[(m-k)^2+(n-l)^2]^2} \end{aligned} \tag{11}$$

Inserting B_1, B_2, B_3 and B_4 in Eq. (10) , we obtain:

$$\begin{aligned} F_p = {} & \frac{E\alpha^2}{4} \\ & \sum_{m=1}^{M}\sum_{n=1}^{N}\sum_{k=1}^{K}\sum_{l=1}^{L}\left\{ \frac{A_{mn}A_{kl}ml(nk-ml)-A_{kl}A_{0mn}(nk-ml)^2}{[(m+k)^2+(n+l)^2]^2}\times cx(m+k)cy(n+l)\right. \\ & + \frac{A_{mn}A_{kl}ml(nk+ml)+A_{kl}A_{0mn}(nk+ml)^2}{[(m+k)^2+(n-l)^2]^2}\times cx(m+k)cy(n-l) \\ & + \frac{A_{mn}A_{kl}ml(nk+ml)+A_{kl}A_{0mn}(nk+ml)^2}{[(m-k)^2+(n+l)^2]^2}\times cx(m-k)cy(n+l) \\ & \left. + \frac{A_{mn}A_{kl}ml(nk-ml)-A_{kl}A_{0mn}(nk-ml)^2}{[(m-k)^2+(n-l)^2]^2}\times cx(m-k)cy(n-l)\right\} \end{aligned} \tag{12}$$

Then, the Airy stress function F can be obtained by

$$F = F_h + F_P \tag{13}$$

It is evident from Eq. (7), Eq. (12) and Eq. (13) that F is a second order function with regard to the unknown deflection coefficients A_{mn}. To compute the unknown coefficients A_{mn}, the global Galerkin method is applied to the equilibrium Eq. (1),

$$\iiint_v \varphi(x,y,z)sx(i)sy(j)dxdydz = 0, \qquad i = 1,2,3... \quad j = 1,2,3... \tag{14}$$

Upon substituting Eq. (13) into Eq. (1), and then Eq. (1) to Eq. (14) after a lengthy derivation, we obtain a system of third order coupled NAEs, with respect to the unknown coefficients A_{mn}, the expression of the derived NAEs is

$$\begin{aligned}
&\sum_{m=1}^{M}\sum_{n=1}^{N} A_{mn} \times D\pi^4 (\frac{m^2}{a^2} + \frac{n^2}{b^2})^2 H_{01}(i,j,m,n) \\
&+ \sum_{m=1}^{M}\sum_{n=1}^{N}\sum_{k=1}^{K}\sum_{l=1}^{L}\sum_{r=1}^{R}\sum_{s=1}^{S} A_{mn}A_{kl}A_{rs} \times (-t) \\
&\frac{E\alpha^2\pi^4}{4a^2b^2}(H_1 + H_2 + H_3 + H_4 - 2H_9 - 2H_{10} - 2H_{11} - 2H_{12}) \\
&+ \sum_{m=1}^{M}\sum_{n=1}^{N}\sum_{k=1}^{K}\sum_{l=1}^{L} A_{mn}A_{kl} \times (-t) \\
&\frac{E\alpha^2\pi^4}{4a^2b^2}\sum_{r=1}^{R}\sum_{s=1}^{S} A_{0rs}(H_1 + H_2 + H_3 + H_4 - 2H_9 - 2H_{10} - 2H_{11} - 2H_{12}) \\
&+ \sum_{k=1}^{K}\sum_{l=1}^{L}\sum_{r=1}^{R}\sum_{s=1}^{S} A_{kl}A_{rs} \times (-t) \\
&\frac{E\alpha^2\pi^4}{4a^2b^2}\sum_{m=1}^{M}\sum_{n=1}^{N} A_{0mn}(H_6 + H_7 - H_5 - H_8 + 2H_{13} - 2H_{14} - 2H_{15} + 2H_{16}) \\
&+ \sum_{k=1}^{K}\sum_{l=1}^{L} A_{kl} \times (-t) \\
&\frac{E\alpha^2\pi^4}{4a^2b^2}\sum_{m=1}^{M}\sum_{n=1}^{N}\sum_{r=1}^{R}\sum_{s=1}^{S} A_{0mn}A_{0rs}(H_6 + H_7 - H_5 - H_8 + 2H_{13} - 2H_{14} - 2H_{15} + 2H_{16})
\end{aligned} \tag{15}$$

$$
\begin{aligned}
&+\sum_{m=1}^{M}\sum_{n=1}^{N} A_{mn}\times(-t)\\
&\left\{\frac{m^2\pi^2}{a^2}\left[\left(\frac{P_x}{bt}+\sigma_{rx}-\frac{6}{b^2t}M_x\right)H_{01}(i,j,m,n)+\frac{12}{b^3t}M_xH_{03}(i,j,m,n)\right]\right.\\
&+\frac{n^2\pi^2}{b^2}\left[\left(\frac{P_y}{at}+\sigma_{ry}-\frac{6}{a^2t}M_y\right)H_{01}(i,j,m,n)+\frac{12}{a^3t}M_yH_{02}(i,j,m,n)\right]\\
&\left.+\frac{2\tau\pi^2}{ab}mn\times H_{04}(i,j,m,n)\right\}\\
&+\sum_{m=1}^{M}\sum_{n=1}^{N} A_{0mn}\times(-t)\\
&\left\{\frac{m^2\pi^2}{a^2}\left[\left(\frac{P_x}{bt}+\sigma_{rx}-\frac{6}{b^2t}M_x\right)H_{01}(i,j,m,n)+\frac{12}{b^3t}M_xH_{03}(i,j,m,n)\right]\right.\\
&+\frac{n^2\pi^2}{b^2}\left[\left(\frac{P_y}{at}+\sigma_{ry}-\frac{6}{a^2t}M_y\right)H_{01}(i,j,m,n)+\frac{12}{a^3t}M_yH_{02}(i,j,m,n)\right]\\
&\left.+\frac{2\tau\pi^2}{ab}mn\times H_{04}(i,j,m,n)\right\}\\
&-Q\times H_{00}(i,j)=0
\end{aligned}
$$

Where, for simplicity, the coefficient matrix $H_1(i,j,m,n,k,l,r,s)$ is denoted by H_1 and so forth. All the coefficient matrices can be obtained by performing integration over the whole volume of the plate. We can write the Eq. (15) in a matrix form,

$$[K_f]_{MN\times MN}A_f+[K_s]_{MN\times(MN)^2}A_s+[K_t]_{MN\times(MN)^3}A_t+[C]_{MN\times 1}=0 \tag{16}$$

Where $[C]_{MN\times 1}$ is the constant column matrix, $[K_f]_{MN\times MN}$, $[K_s]_{MN\times(MN)^2}$ and $[K_t]_{MN\times(MN)^3}$ are the first order, second order, third order coefficient matrices, respectively, with their subscripts being their dimensions. A_f, A_s, A_t are the first order, second order and third order unknown vectors, respectively. The exact descriptions of the matrices and vectors in Eq. (16) are provided in the paper by Dai, Paik and Atluri (2011a).

We can see from Eq. (16) that the number of nonlinear terms of the NAEs becomes larger dramatically with the increase of deflection function terms $M\times N$. For instance, if we take $M=N=2$, $M=N=3$, $M=N=4$ and $M=N=5$ the number of third order terms in one equation is 64, 729, 4096 and 15625, respectively. Therefore, solving the system of third order simultaneous equations to solve for the coefficients A_{MN} normally requires a large amount of computational efforts, especially when $M\times N$ are not small. Moreover, since the solution of each coefficient should be unique, one will have to construct a suitable initial guess for the

NAEs to find the one physical solution among the multiple solutions. Because of these two reasons, it has been considered to be an impossible task to solve such a set of highly nonlinear third order simultaneous equations [Paik, Thayamballi, Lee and Kang 2001].

In section 3, an extraordinarily efficient optimal vector-driven algorithm, which can be used to iteratively and efficiently solve a large set of NAEs, is introduced. This algorithm is shown to be several orders of magnitude faster than the exponentially convergent scalar homotopy algorithm (ECSHA) used in the earlier paper [Dai, Paik and Atluri (2011a)]. In section 4, approaches for providing the proper initial guess to directly solve the highly nonlinear algebraic equations are discussed.

3 The Optimal Vector-Driven Algorithm

The thoroughly novel optimal vector-driven algorithm, which is recently proposed by Liu and Atluri (2011b), is based on an invariant manifold defined in the space of (x, t) in terms of the residual-norm of the vector $\mathbf{F}(\mathbf{x})$. Although they start from a continuous invariant manifold based on the residual-norm and arrive at a system of vector-driven ODEs to govern the evolution of unknown variables, interestingly they finally derive a novel algorithm of purely iterative type in nature without resorting on the fictitious time and its step size. Liu and Atluri (2011b) point out and prove that the OVDA is convergent automatically, easy to implement, and without calculating the inversions of the Jacobian matrices. The advantages make the OVDA an efficient tool to solve a large set of NAEs.

3.1 Newton method and scalar homotopy method

Before introducing the OVDA, we first consider the following NAEs:

$$\begin{aligned} &\mathbf{F}(\mathbf{x}) = \mathbf{0}, \\ &\textit{where } \mathbf{x} = (x_1, x_2, ..., x_n)^T, \textit{ and } \mathbf{F} = (F_1, F_2, ..., F_n)^T \end{aligned} \tag{17}$$

Traditionally, the classic Newton-Raphson method for solving these NAEs is given by

$$\mathbf{x}^{k+1} = \mathbf{x}^k - \mathbf{B}^{-1}(\mathbf{x}^k)\mathbf{F}(\mathbf{x}^k) \tag{18}$$

Where $\mathbf{B}$ denotes the Jacobian matrix of $\mathbf{F}(\mathbf{x})$, and $\mathbf{x}^{k+1}$ is the $(k+1)th$ iteration for $\mathbf{x}$. Newton's method has an advantage, in that it is quadratically convergent. However, its convergence depends on the initial guess of the solution. If the initial guess is beyond the attracting zone, the Newton's method fails. In addition, in Newton's method it is numerically expensive to compute the inverse of the Jacobian matrix at every iteration step.

Many contributions have been made to avoid the shortcomings of Newton's method. Davidenko (1953) first developed a homotopy method to solve NAEs by numerically integrating $\dot{\mathbf{x}}(t) = -\mathbf{H}_{\mathbf{x}}^{-1}\mathbf{H}_{\mathbf{t}}(\mathbf{x},t), \quad \mathbf{x}(\mathbf{0}) = \mathbf{a}$, where $\mathbf{H}$ is a vector homotopy function. Thus, it is called a vector homotopy method. This vector homotopy method is global convergent. However, it suffers a slow convergence speed due to the inverse of Jacobian matrix and a required small time step.

To take advantage of the global convergence of the homotopy method and also to avoid computing the inverse of the Jacobian matrix, the scalar homotopy method (SHM), was developed by Liu, Yeih, Kuo and Atluri (2009). In their study, instead of using a vector function, they introduced a scalar function

$$h(\mathbf{x},t) = \frac{1}{2}\left[t\left\|\mathbf{F}(\mathbf{x})\right\|^2 - (1-t)\left\|\mathbf{x}-\mathbf{a}\right\|^2\right] = 0 \tag{19}$$

Based on this scalar function and the consistency condition, they derived the following evolution equation:

$$\dot{\mathbf{x}} = -\frac{\frac{\partial h}{\partial t}}{\left\|\frac{\partial h}{\partial \mathbf{x}}\right\|^2}\frac{\partial h}{\partial \mathbf{x}} \tag{20}$$

Where

$$\frac{\partial h}{\partial t} = \frac{1}{2}\left[\left\|\mathbf{F}(\mathbf{x})\right\|^2 + \left\|\mathbf{x}\right\|^2\right] \tag{21}$$

$$\frac{\partial h}{\partial \mathbf{x}} = t\mathbf{B}^{\mathbf{T}}\mathbf{F} - (1-t)\,\mathbf{x} \tag{22}$$

The scalar homotopy method basically aims to construct a path from the solution of the auxiliary scalar function to the solution of the desired function continuously. The SHM shows many merits to deal with a variety of problems [Liu, Yeih, Kuo and Atluri (2009), Fan, Liu, Yeih and Chan (2010)]. Furthermore, Liu, Ku, Yeih and Atluri (2011) combined this idea with an exponentially convergent scalar homotopy function, and developed a manifold-based exponentially convergent scalar homotopy method (ECSHA) [Liu, Ku, Yeih, Fan and Atluri (2011)]. The ECHSA shows a better performance in solving a large system of NAEs. The evolution equation of the ECSHA is:

$$\dot{\mathbf{x}} = \frac{-v}{2(1+t)^m}\frac{\left\|\mathbf{F}(\mathbf{x})\right\|^2}{\left\|\mathbf{B}^{\mathbf{T}}\mathbf{F}(\mathbf{x})\right\|^2}\mathbf{B}^{\mathbf{T}}\mathbf{F}(\mathbf{x}) \tag{23}$$

However, the ECHSA is not faultless. Two major drawbacks appear in the ECSHA: irregular bursts and flattened behavior appearing in the trajectory of the residual-error (Numerical illustrations in section 5 confirm these drawbacks).

3.2 Optimal vector-driven method

Recently, Liu and Atluri (2011b) overcame the limitations of the residual-norm based algorithms, and proposed a thoroughly novel optimal vector-driven algorithm, of purely iterative nature, which can be easily implemented to solve nonlinear algebraic equations (NAEs). In the work by Liu and Atluri (2011b), they start from a continuous manifold defined in terms of a residual-norm, and arrive at a system of ODEs driven by a vector, which is a combination of residual vector and gradient vector. Then a scalar equation is derived to keep the discretely iterative orbit on the manifold. Finally, two parameters—bifurcation parameter γ and optimal α are introduced, which guarantee the automatic convergence of the residual error.

To begin with, they formulate a scalar Newton homotopy function for the nonlinear algebraic equations in Eq. (17):

$$h(\mathbf{x},t)=\frac{1}{2}Q(t)\left\|\mathbf{F}(\mathbf{x})\right\|^2-\frac{1}{2}\left\|\mathbf{F}(\mathbf{x}_0)\right\|^2=0 \tag{24}$$

Where, $\mathbf{x}$ is a function of a fictitious time-like variable t, and its initial value is $\mathbf{x}(0)=\mathbf{x}_0$. When $Q>0$, the dynamical system $h(\mathbf{x}(t),t)=0$ makes sense. Hence, differentiate the Eq. (24) with respect to t, obtaining

$$\frac{1}{2}\dot{Q}(t)\left\|\mathbf{F}(\mathbf{x})\right\|^2+Q(t)(\mathbf{B}^{\mathbf{T}}\mathbf{F})\cdot\dot{\mathbf{x}}=0 \tag{25}$$

We suppose that the evolution of $\mathbf{x}$ is driven by a vector $\mathbf{u}$, that is

$$\dot{\mathbf{x}}=\lambda\mathbf{u} \tag{26}$$

Where,

$$\mathbf{u}=\alpha\mathbf{F}+(1-\alpha)\mathbf{B}^{\mathrm{T}}\mathbf{F} \tag{27}$$

We can see that vector $\mathbf{u}$ is a combination of the residual vector $\mathbf{F}$ and the gradient vector $\mathbf{B}^{\mathrm{T}}\mathbf{F}$. Upon substituting Eq. (26) to Eq. (24), we have

$$\dot{\mathbf{x}}=-q(t)\frac{\left\|\mathbf{F}\right\|^2}{\mathbf{F}^{\mathbf{T}}\mathbf{v}}\mathbf{u} \tag{28}$$

Where

$$\mathbf{A}=\mathbf{B}\mathbf{B}^{\mathrm{T}} \tag{29}$$

$$\mathbf{v}=\mathbf{B}\mathbf{u}=\mathbf{v}_1+\alpha\mathbf{v}_2=\mathbf{A}\mathbf{F}+\alpha(\mathbf{B}-\mathbf{A})\mathbf{F} \tag{30}$$

$$q(t) = \frac{\dot{Q}(t)}{2Q(t)} \tag{31}$$

Therefore, in the present algorithm, once the $Q(t)$ is guaranteed to be monotonically increasing with time t, we may have an absolutely convergent property in solving the NAEs as below:

$$\|\mathbf{F}(\mathbf{x})\|^2 = \frac{\|\mathbf{F}(\mathbf{x}_0)\|^2}{Q(t)} \tag{32}$$

From Eq. (32), we can see that if the $Q(t)$ is chosen to be a monotonically increasing function of t, when t is large, the above equation will enforce the residual error to vanish. In this situation, the approximate solution of $\mathbf{x}$ will be obtained.

However, we expect to derive a discrete time dynamics system in order to perform the numerical iteration. Therefore, the continuous time dynamics system of Eq. (28) is discretized into a discrete time dynamics system by applying Euler scheme

$$\mathbf{x}(t+\Delta t) = \mathbf{x}(t) - \beta \frac{\|\mathbf{F}\|^2}{\mathbf{F^T v}}\mathbf{u} \tag{33}$$

Where

$$\beta = q(t)\Delta t \tag{34}$$

is the steplength. In order to keep $\mathbf{x}$ on the manifold of Eq. (32), we can consider the evolution of $\mathbf{F}$ along the path $\mathbf{x}(t)$, which represents

$$\dot{\mathbf{F}} = \mathbf{B}\dot{\mathbf{x}} = -q(t)\frac{\|\mathbf{F}\|^2}{\mathbf{F^T v}}\mathbf{v} \tag{35}$$

Or transforming into a discrete form by applying Euler scheme,

$$\mathbf{F}(t+\Delta t) = \mathbf{F}(t) - \beta \frac{\|\mathbf{F}\|^2}{\mathbf{F^T v}}\mathbf{v} \tag{36}$$

Taking the square-norms of both sides of Eq. (36), and using Eq. (32) we obtain

$$\frac{C}{Q(t+\Delta t)} = \frac{C}{Q(t)} - 2\beta\frac{C}{Q(t)} + \beta^2 \frac{C}{Q(t)}\frac{\|\mathbf{F}\|^2}{(\mathbf{F^T v})^2}\|\mathbf{v}\|^2 \tag{37}$$

Thus, we can derive the following scalar equation

$$a_0\beta^2 - 2\beta + 1 - \frac{Q(t)}{Q(t+\Delta t)} = 0 \tag{38}$$

Where

$$a_0 = \frac{\|\mathbf{F}\|^2 \|\mathbf{v}\|^2}{(\mathbf{F}^{\mathbf{T}}\mathbf{v})^2} \tag{39}$$

As a result, the discrete time dynamical system $h(\mathbf{x}(t),t) = 0$ remains to be an invariant manifold in the space of $(\mathbf{x},t)$.

Now, we specify the discrete time dynamics $h(\mathbf{x}(t),t) = 0$, $t \in \{0,1,2...\}$, through specifying the discrete time dynamics $Q(t)$, $t \in \{0,1,2...\}$. Note that the discrete time dynamics is an iterative dynamics which amounts to an iterative algorithm.

Let

$$s = \frac{Q(t)}{Q(t+\Delta t)} = \frac{\|F(\mathbf{x}(t+\Delta t))\|^2}{\|F(\mathbf{x}(t))\|^2} \tag{40}$$

Which is an important quantity to assess the convergence property of numerical algorithm for solving NAEs. From Eq. (38) and Eq. (40), we can derive

$$a_0\beta^2 - 2\beta + 1 - s = 0 \tag{41}$$

From Eq. (39) we know $a_0 \geq 1$ (Cauchy-Schwarz inequality). If we let

$$1 - (1-s)a_0 = \gamma^2 \geq 0, \ (so\ that\ \ s = 1 - \frac{1-\gamma^2}{a_0}) \tag{42}$$

Then we can solve the Eq. (41), and obtain

$$\beta = \frac{1 - \sqrt{1-(1-s)a_0}}{a_0} = \frac{1-\gamma}{a_0} \tag{43}$$

and from Eqs. (33) and (39) we can derive the following algorithm

$$\mathbf{x}(t+\Delta t) = \mathbf{x}(t) - (1-\gamma)\frac{\mathbf{F}^{\mathbf{T}}\mathbf{v}}{\|\mathbf{v}\|^2}\mathbf{u} \tag{44}$$

Where $0 \leq \gamma < 1$ is a bifurcation parameter enabling us to switch the slow convergence to a new situation wherein the residual-error is quickly decreased. Eqs. (40) and (42) prove that

$$\frac{\|F(\mathbf{x}(t+\Delta t))\|}{\|F(\mathbf{x}(t))\|} = \sqrt{s} < 1 \tag{45}$$

which guarantees the new algorithm to be absolutely convergent to the true solution.

Until now, the parameter α in Eq. (27) is still undetermined. The algorithm Eq. (44) does not specify how to choose α. One simple way is to choose the parameter α by user. However, make a closer investigation, we can determine a suitable α to minimize s (see Eq. (42)). Since Eq. (45) indicates that a smaller s may speed up the convergence. Upon inserting Eq. (39) to Eq. (42), we obtain

$$s = 1 - \frac{(1-\gamma^2)(\mathbf{F}\cdot\mathbf{v})^2}{\|\mathbf{F}\|^2 \|\mathbf{v}\|^2} \tag{46}$$

As we wrote in Eq. (30), $\mathbf{v}$ is defined to include the parameter α. Therefore, let $\partial s/\partial\alpha = 0$, we can obtain

$$\alpha = \frac{(\mathbf{v}_1\cdot\mathbf{F})(\mathbf{v}_1\cdot\mathbf{v}_2) - (\mathbf{v}_2\cdot\mathbf{F})\|\mathbf{v}_1\|^2}{(\mathbf{v}_2\cdot\mathbf{F})(\mathbf{v}_1\cdot\mathbf{v}_2) - (\mathbf{v}_1\cdot\mathbf{F})\|\mathbf{v}_2\|^2} \tag{47}$$

The parameter α can be called the optimal α, because it can bring us a new strategy to select the best orientation to search the solution of NAEs. Furthermore, we have an explicit form of optimal α which can be easy to implement in numerical program.

Since the fictitious time is now discrete, we finally get a purely iterative optimal vector-driven algorithm (OVDA) by Eq. (44):

Select $0 \le \gamma < 1$, and give an initial guess value $\mathbf{x}_0$ for the vector.

For $k = 0, 1, 2...$ repeat the following procedures

$$\mathbf{v}_1^k = \mathbf{A}_k\mathbf{F}_k \tag{48}$$

$$\mathbf{v}_2^k = (\mathbf{B}_k - \mathbf{A}_k)\mathbf{F}_k \tag{49}$$

$$\alpha_k = \frac{\left[\mathbf{v}_1^k, \mathbf{v}_2^k, \mathbf{F}_k\right]\cdot\mathbf{v}_1^k}{\left[\mathbf{v}_2^k, \mathbf{v}_1^k, \mathbf{F}_k\right]\cdot\mathbf{v}_2^k} \tag{50}$$

$$\mathbf{u}_k = \alpha_k\mathbf{F}_k + (1-\alpha_k)\mathbf{B}_k^{\mathrm{T}}\mathbf{F}_k \tag{51}$$

$$\mathbf{v}_k = \mathbf{B}_k\mathbf{u}_k \tag{52}$$

$$\mathbf{x}_{k+1} = \mathbf{x}_k - (1-\gamma)\frac{\mathbf{F}_k^{\mathrm{T}}\mathbf{v}_k}{\|\mathbf{v}_k\|^2}\mathbf{u}_k \tag{53}$$

If $\mathbf{x}_{k+1}$ converges to a given stopping criterion $\|\mathbf{F}_{k+1}\| < \varepsilon$, then stop; otherwise repeat (ii). Where $\mathbf{B}$ is the Jacobian matrix of $\mathbf{F}(\mathbf{x})$, $\mathbf{A}$ is $\mathbf{B}\mathbf{B}^{\mathrm{T}}$ by definition, α_k is an elegant Jordan algebra form of Eq. (47).

In summary, a thoroughly novel algorithm is given above for solving NAEs. In the present OVDA [Liu and Atluri (2011b)], the parameter γ is a very important factor,

which is a bifurcation parameter and enables us to switch the slow convergence to a new situation wherein the residual-error is quickly decreased. The optimal parameter of α was derived exactly in terms of a Jordan algebra, and thus it is very time saving to implement the optimization technique into the numerical program. Therefore, for the novel OVDA, we have two mechanisms γ and α to accelerate the convergence speed of the residual error of the NAEs. Specifically, the bifurcation parameter γ should be chosen according to the given NAEs, while the optimization parameter α will be exactly calculated according to every iteration step (see Eq. (50)). The optimal α can bring us a new strategy to select the best orientation to search the solution of NAEs in every iteration step. In application, since the suitable bifurcation parameter γ is not a constant value, we set γ to be zero in every example. Although we use only one mechanism to speed up the convergence speed in the illustrations, the OVDA with optimal parameter α still shows a much better performance than the ECSHA.

4 Selection of the Initial Guess Solution

When an iterative method is employed to solve the NAEs, the initial guess of the solution is of great importance. In general, when an initial guess is in the vicinity of a solution, it may significantly reduce the number of iterations and also avoid deviating from the current solution. Consider a simple case, a rectangular plate subjected to uniaxial compression load P. The Eq. (16) is its governing equations.

When P is small compared with P_{cr}, the linear terms of Eq. (16) play a dominate role in the whole equation since the deflection is small and the nonlinear terms can be quite small. Based on this observation, one can throw off the nonlinear terms in Eq. (16), and solve the linear part of the NAEs quite easily. Intuitively, the solution of the linear equations is taken as a reasonable initial guess for the NAEs, when the applied loads are small. However, with the increase of P, the nonlinear terms grow large quickly. When it reaches a certain level, the magnitude of the nonlinear terms becomes comparable to that of the linear terms. Thus, the solution of the linear equations may not be a good initial guess any more. Therefore, this approach fails when the plate deflects finitely.

Another approach to construct a proper initial guess for the NAEs is to take the solution of the last load step as the initial guess of the current step when the two loads are reasonably close to each other. For instance, we can use the solution of the NAEs with load P as the initial guess for the NAEs with load $P+\Delta P$ where ΔP is relatively small compared with P. It makes sense since a small change of the load will results in a small change of the deflection, thus, a small difference between the solutions. This approach makes use of the approximation between solutions of two close loads. Theoretically, this load-tracking approach is applicable to any

situation when the plate deflects finitely so we use this approach to keep track of the physical solution in each load step in the numerical illustrations. Although we take the compression load as an example, this approach still makes sense when the plate is subjected to a combination of loading conditions. In practical applications, we employ the load-tracking approach to provide the initial guess for the NAEs with $M \times N$ terms to keep track of the physical solutions.

5 Numerical illustrations

In this section, several numerical examples are provided to demonstrate efficiency of the optimal vector-driven algorithm (OVDA) by comparing it with the exponentially convergent scalar homotopy algorithm (ECSHA). In addition, the accuracy of the proposed global nonlinear Galerkin method, which is applying the global Galerkin method directly to the highly nonlinear PDEs and directly solving the resultant NAEs at every load step, is also validated. These examples make the global nonlinear Galerkin method, the current state-of-science in symbolic computation, and algorithms for directly solving the NAEs such as the OVDA presented in this paper, as viable tools for solving nonlinear structural mechanics problems. Also, because of the extremely high accuracy provided at a very modest cost, the methods presented in this paper may also provide the much needed highly accurate benchmark solutions against which other numerical methods may be validated.

In the following examples, the Young's modulus and Poisson's ratio are assumed to be $E = 205.8\ GPa$ and $\upsilon = 0.3$, respectively. For applying the OVDA, the parameter γ is set to be 0 in all examples. The parameter may influence the convergence property of the OVDA, which as mentioned above is a bifurcation parameter that enables us to switch the slow convergence to a new situation that the residual error is quickly decreased. Since the NAEs are changing with the applied load, the suitable bifurcation parameter is always changing, for simplicity we set γ to be zero.

5.1 A square plate under uniaxial compression

In this example, a simply supported square plate under uniaxial compression is analyzed. The dimensions of this plate are $a = 1$, $b = 1$, $t = 0.009$, where a, b, t represent length, width and thickness respectively. All dimensions in this study are in metres unless otherwise mentioned. According to Eq. (4) and Eq. (5), the initial deflection is assumed to consist of $M \times N$ terms,

$$w_0 = \sum_{m=1}^{M} \sum_{n=1}^{N} A_{0mn} sx(m) sy(n)$$

Where, A_{0mn} are the known coefficients with A_{011} being 0.45×10^{-3} and other elements being zeros. The deflection function with $M \times N$ terms is,

$$w = \sum_{m=1}^{M} \sum_{n=1}^{N} A_{mn} sx(m) sy(n)$$

The global Galerkin method is applied to deal with five cases wherein the deflection functions are assumed with 1×1 term, 2×2 terms, 3×3 terms, 4×4 terms and 5×5 terms, respectively. A case of the incremental global Galerkin method developed by Ueda, Rashed and Paik (1987) is used to compare with the present global direct nonlinear Galerkin method. Figure 1 displays curves that plot the compression load against the maximum deflection of the plate. The compression load acting on the plate varies from 0 to 2 (P_{cr}) with load step being 0.1. Therefore, for each case, there are 20 load steps (if we exclude load=0), hence 20 sets of NAEs to solve.

It may be seen from Figure 1 that the results of the present nonlinear global Galerkin method and the incremental global Galerkin method are in good agreement. Figure 1 also provides the comparison of the results of the present global nonlinear Galerkin method with different order trigonometric functions. We only plot three of the five cases for sake of visual clarity. We can see that all the three cases with 1×1, 3×3 and 5×5 terms are in very good agreement, which confirms the accuracy of the global nonlinear Galerkin method.

Table 2 provides the sizes of NAEs of different cases. We see from Table 2 that the number of nonlinear terms in the NAEs becomes large dramatically with the increase of the number of terms of the deflection function. The OVDA is employed to solve the resultant sets of NAEs and the load-tracking approach is adopted to provide the initial guess.

Table 3 gives the comparison of the iteration numbers and computational time for solving1×1, 2×2, 3×3, 4×4, and 5×5 cases by using OVDA and ECSHA in MATLB. It can be seen that the computational effort of the OVDA for solving the resultant NAEs is several times less than that of the ECSHA. For example, for the case with 3×3 terms, the effort of solving 20 sets of NAEs by using OVDA is 1911 steps and 621.7s compared with the ECSHA which requires up to 24302 steps and 5969.17s (both in PC Core2). The results given indicate that the OVDA is roughly 10-20 times faster than the ECSHA in the sense of iteration numbers, when the system of NAEs is not small ($M \times N \geq 4$).

To further investigate the convergence trajectory of the residual-error of the optimal vector-driven algorithm, we take out the cases with 2×2 terms for example. As we mentioned above, the external load is applied to the plate through 20 steps

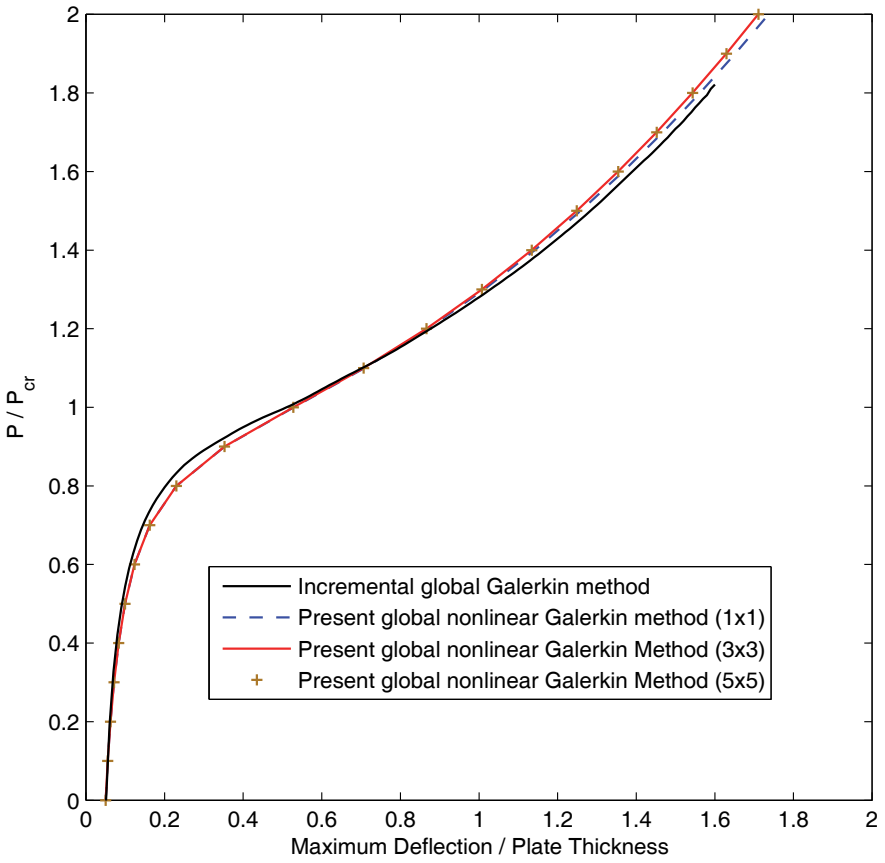

Figure 1: Comparison of the load-deflection curves for the present global nonlinear Galerkin method and the incremental global Galerkin method

which correspond to 20 sets of NAEs. Without losing generality, we investigate the residual error of the OVDA of the 10^{th} set of NAEs by comparing with the ECHSA.

Figure 2 shows that the convergence rate of the OVDA is much steeper and direct. While for the ECSHA, the residual-error trajectory zigzags its way full of twists and turns, which verifies the two major drawbacks of the ECSHA as we mentioned in section 3: irregular bursts and flattened behavior in the trajectory of residual error. Specifically, for solving the present system of NAEs corresponding to the 10^{th} load step (M=2, N=2; load =1), the iteration numbers by using ECSHA and OVDA are 711 and 40 respectively (ratio 17.78). The results confirm the high efficiency of the

Table 2: The sizes of the NAEs

Cases$(M \times N)$	N_{eqs}	N_{3th}	N_{2th}	N_{1th}
1×1	1	1	1	1
2×2	4	64	16	4
3×3	9	729	81	9
4×4	16	4096	256	16
5×5	25	15625	625	25
$N_{eqs}$is the number of equations; N_{1th} N_{2th} N_{3th} are the number of first order terms, second order terms and third order terms, respectively in one equation.				

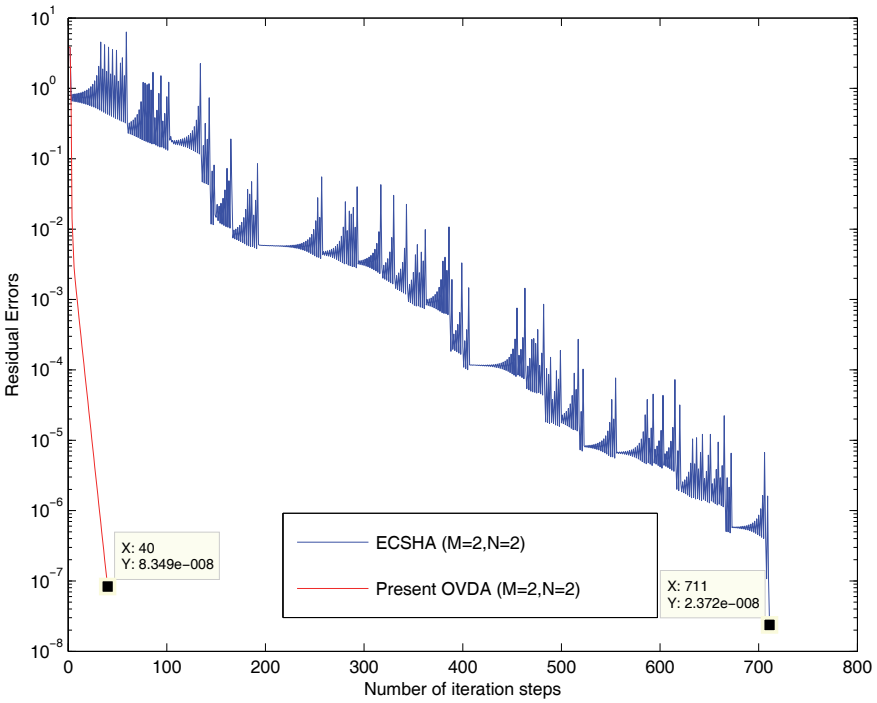

Figure 2: Comparison of the residual-error trajectory for solving the NAEs corresponding to M=2, N=2 and load=1 by the OVDA and the ECSHA in the case of a square plate under uniaxial compression

Table 3: Comparison of the computational efforts for OVDA and ECSHA

Cases$(M \times N)$	ε	N_{it}^{ECSHA}	N_{it}^{OVDA}	R_{Nit}	T^{ECSHA}	T^{OVDA}	R_T
1×1	10^{-7}	106	71	1.49	8.38s	7.32s	1.14
2×2	10^{-7}	3833	185	20.72	70.70s	27.6s	2.56
3×3	10^{-5}	24302	1911	12.72	5969.17s	621. 7s	9.60
4×4	10^{-5}	83483	8362	9.98	224680.00s	22479.8s	9.99
5×5	10^{-3}	95094	4561	20.85	2375733.68s	85068.2s	27.93
$\varepsilon$is the convergence criterion; N_{it} is the number of total iterations; T is the computational time for solving 20 sets of NAEs. R_{Nit} is the ratio of the iteration number of ECSHA to the iteration number of OVDA. R_T is the ratio of the computing time of ECSHA to that of OVDA.							

OVDA.

5.2 A rectangular plate under uniaxial compression

In this example, a simply supported rectangular plate under uniaxial compression is considered. Its dimensions are $a = 1.68$, $b = 0.98$, $t = 0.011$. The pattern of the initial deflection and the deflection function is given by Eq. (4) and Eq. (5). Here $A_{0mn} = 0$ is taken except $A_{011} = 1.1 \times 10^{-3}$ and $A_{021} = 0.22 \times 10^{-3}$. The present global nonlinear Galerkin method is applied to solve this rectangular plate under uniaxial compression. For comparison the analysis is also carried out by the FEM using rectangular, four node, and nonconforming plate elements with five degrees freedom at each node; 7×18 elements for half of the plate [Ueda, Rashed and Paik 1987]. Figure 3 displays curves that plot the compression load against the deflections of two points A and B whose positions are $(0.25a,\ 0.5b)$ and $(0.75a,\ 0.5b)$ respectively, if we set the lower left corner of the plate $(0,\ 0)$ and upper right corner $(a,\ b)$.

It may be seen from Figure 3 that the results of the present global nonlinear Galerkin method and that of the tangent stiffness FEM are in good agreement, which confirms the accuracy of the global nonlinear Galerkin method. Table 4 provides the computational information of the OVDA and the ECSHA for solving the NAEs. The applied loads are 0:1:7 and 8:0.5:14 and 15:1:18 in this example. Thus, there are 24 load steps (if we exclude load=0) and correspondingly 24 sets of NAEs to solve.

Table 4 gives the comparison of the iteration numbers and computational time for solving 2×1, 2×2, 3×2 and 3×3 cases by using OVDA and ECSHA. It can be seen from Table 4 that the computational effort of OVDA for solving the resultant NAEs is much less than that of ECSHA. In general, we see again that the computational effort of the iterations of the OVDA is roughly ten to twenty times less than that of the ECSHA for solving even 9 NAEs. As the number of NAEs increases, OVDA can be seen to be several orders of magnitude faster than ECSHA. To closely investigate the property of the two methods, we plot the curve of the residual-error trajectory of the current set of NAEs, which corresponds to the load=9 (M=3, N=2).

Figure 4 shows that the convergence trajectory of the OVDA is much steeper and direct than that of the ECSHA. Specifically, for solving the present system of NAEs corresponding to load=9 (M=3, N=2), the iteration numbers by using the ECSHA and the OVDA are 1312 and 73 respectively, which verifies the high efficiency of the OVDA. For the particular set of NAEs, the ratio of the number of iterations between OVDA and ECSHA is 17.97. In summary, the results obtained confirm the accuracy and efficiency of the present scheme in the case of rectangular plates.

Table 4: Comparison of the computational efforts for OVDA and ECSHA

				Number of iterations			Computing time		
Cases$(M \times N)$	ε	N_{eqs}	N_{3th}	N_{it}^{ECSHA}	N_{it}^{OVDA}	R_{Nit}	T^{ECSHA}	T^{OVDA}	R_T
2×1	10^{-7}	2	8	595	90	6.61	2.41s	1.53s	1.58
2×2	10^{-7}	4	64	10556	446	23.67	133.8s	12.5s	10.70
3×2	10^{-5}	6	216	14176	910	15.58	658.5s	68.9s	9.56
3×3	10^{-5}	9	729	54110	3097	17.47	13683.6s	943.8s	14.50

Table 5: Comparison of the computational efforts for OVDA and ECSHA

				Number of iterations			Computing time		
Cases$(M \times N)$	ε	N_{eqs}	N_{3th}	N_{it}^{ECSHA}	N_{it}^{OVDA}	R_{Nit}	T^{ECSHA}	T^{OVDA}	R_T
1×1	10^{-10}	1	1	167	83	2.01	11.31s	9.10s	1.24
2×2	10^{-10}	4	64	2297	104	22.09	49.21s	28.54s	1.72
3×3	10^{-5}	9	729	11846	1743	6.80	2638.76s	535.12s	4.93

Table 6: Comparison of the computational efforts for OVDA and ECSHA

				Number of iterations			Computing time		
Cases$(M \times N)$	ε	N_{eqs}	N_{3th}	N_{it}^{ECSHA}	N_{it}^{OVDA}	R_{Nit}	T^{ECSHA}	T^{OVDA}	R_T
1×1	10^{-7}	2	8	153	85	1.80	10.29s	9.03s	1.14
2×2	10^{-7}	4	64	1999	169	11.83	46.57s	29.68s	1.57
3×3	10^{-5}	9	729	21227	1274	16.67	5239.82s	456.56s	11.48

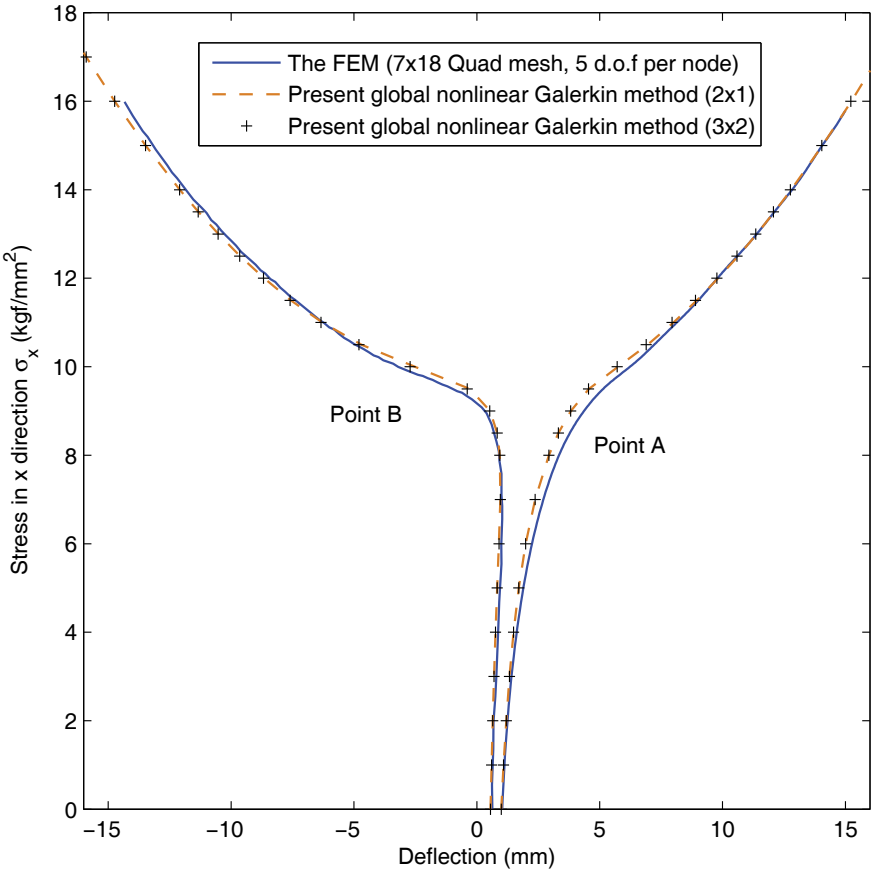

Figure 3: Comparison of the stress versus the deflection of points A and B for the global nonlinear Galerkin method and the finite element method

5.3 A square plate subjected to lateral load

A square plate subjected to a uniformly distributed lateral load Q is considered in this example. Its dimensions are $a = 1$, $b = 1$, $t = 0.009$. The deflection function is in the same pattern as before. The initial deflection is assumed to be zero such that $A_{0mn} = 0$. The present global nonlinear Galerkin method with the aid of optimal vector-driven algorithm to solve NAEs is applied to solve the several cases. The lateral loads are 0:2:50 ($\frac{Et^4}{b^4}$).

The deflection curves of the current global nonlinear Galerkin method and other methods are not given in this example since the accuracy of the proposed global

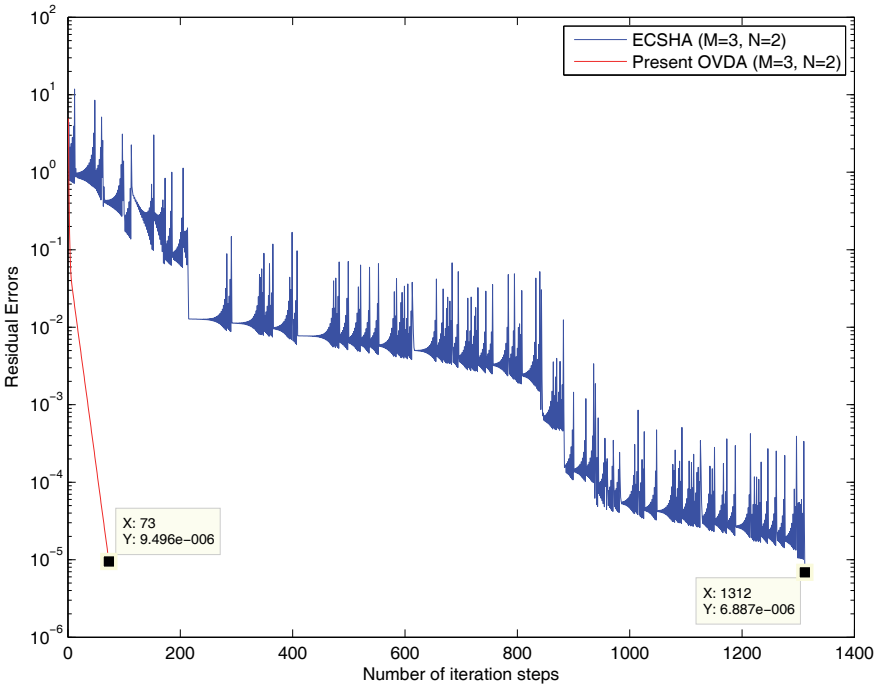

Figure 4: Comparison of the residual-error trajectory for solving the NAEs corresponding to M=3, N=2 and load=9 by the OVDA and the ECSHA in the case of a rectangular plate under uniaxial compression

nonlinear Galerkin method is illustrated in the first two examples as well as the paper by Dai, Paik and Atluri (2011a), and we concentrate on the validation of the efficiency of the OVDA below. Table 5 indicates that the computational effort of the OVDA for solving the same cases is several times less than the ECSHA. Specifically, for solving the present NAEs (M=3, N=3, load=24), the iteration number of the ECSHA is 360, while the iteration number of the OVDA is 69 (ratio 5.22). Figure 5 displays the convergence rate of the two methods, from which we can see that the OVDA is much direct and steeper.

5.4 A square plate subjected to lateral pressure combined with uniaxial compression

In this example, a square plate subjected to lateral pressure combined with uniaxial compression is considered. The compression load acting on the plate is a constant value $0.6P_{cr}$. The lateral pressures acting on the plate are 0:2:50 ($\frac{Et^4}{b^4}$). The di-

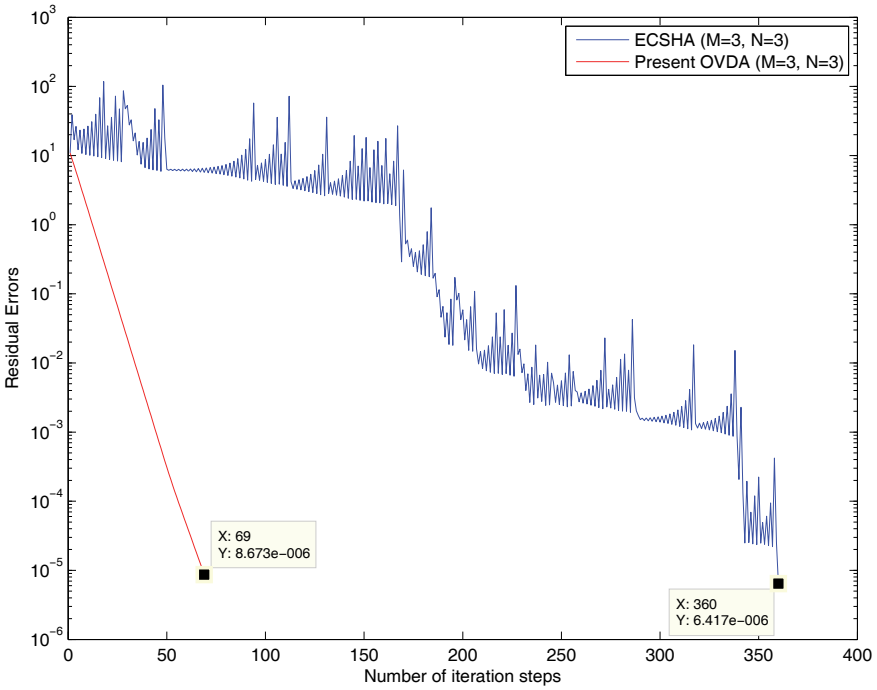

Figure 5: Comparison of the residual-error trajectory for solving the NAEs corresponding to M=3, N=3 and load=24 by the OVDA and the ECSHA in the case of a square plate subjected to lateral load

mensions of the plate are $a = 1$, $b = 1$, $t = 0.02$. The deflection function is in the same form as the above examples. The initial deflection is assumed to be zero. The present global nonlinear Galerkin method with OVDA is applied to solve several cases.

Table 6 provides the results of the computational efforts for the optimal vector-driven algorithm and the exponentially convergent scalar homotopy algorithm in the case of a simply supported square plate subjected to lateral pressure combined with uniaxial compression. It can be seen that the OVDA is roughly 10-20 times faster (iterations) than the ECSHA in this current case. Figure 6 displays the residual-error trajectory of solving the NAEs (M=3, N=3, load=24) for the two methods, from which we can see that the curve of OVDA goes direct and steeper down. The residual-error trajectory of ECSHA oscillates a lot and converges much slower. The iteration number of the ECSHA for the current NAEs is 594, while the iteration number of the OVDA is 36 (ratio 16.50).

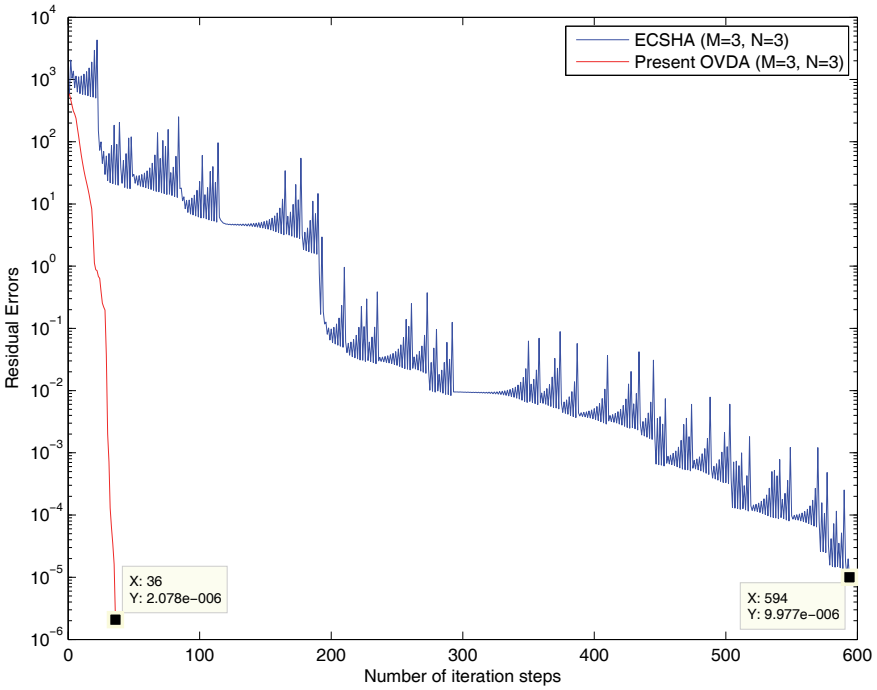

Figure 6: Comparison of the residual-error trajectory for solving the NAEs corresponding to M=3, N=3 and load=24 by the OVDA and the ECSHA in the case of a square plate subjected to lateral pressure combined with uniaxial compression

6 Conclusions

In this paper, the efficiency of the global nonlinear Galerkin method for solving von Karman equations is highly improved by introducing a thoroughly novel optimal vector-driven algorithm (OVDA) [Liu and Atluri (2011b)].

In the global nonlinear Galerkin method, the global Galerkin method is applied directly to the governing highly nonlinear PDEs to derive a system of third order coupled NAEs. The external load is applied incrementally to the plate and the resultant NAEs are solved directly at each load increment. Solving the resultant series of NAEs is thought to be an impossible task until the work by Dai, Paik and Atluri (2011a), where they use the exponentially convergent scalar homotopy algorithm (ECSHA) to solve the series of highly nonlinear third order coupled NAEs. In the present study, a much faster OVDA using $\dot{\mathbf{x}} = \lambda\left[\alpha\mathbf{F} + (1-\alpha)\,\mathbf{B}^{\mathrm{T}}\mathbf{F}\right]$, is employed to solve the series of coupled NAEs. The investigation on the convergence rate of the

residual error is also carried out, which shows that the OVDA has a much steeper and direct convergence trajectory than the ECSHA. Several numerical examples of nonlinear von Karman plates are presented to show that the present algorithm for directly solving the NAEs is several orders of magnitude faster than those in Dai, Paik and Atluri (2011a). In addition, the present global nonlinear Galerkin method yields results which are in excellent agreement with the tangent-stiffness FEM method. However, the FEM requires degrees of freedom which are about two orders of magnitude larger in number than the number of coupled NAEs in the present nonlinear global Galerkin method.

In summary, the efficiency of recently developed methods (such as the present OVDA which can directly solve NAEs without inverting Jacobian matrices) and the state of the science in symbolic computation makes the resurgence of simple global Galerkin methods, as alternatives to the finite element method, to directly solve nonlinear structural mechanics problems without piecewise linear formulations, entirely feasible. Also, because of the extremely high accuracy provided at a very modest cost, the method presented in this paper may also provide the much needed highly accurate benchmark solutions against which other numerical methods may be validated.

Acknowledgement: The first author gratefully acknowledges the support from the China Scholarship Council and the support from college of astronautics in NPU. At UCI, this research was supported by the Army Research Laboratory, with Drs. A. Ghoshal and Dy Le as the Program Officials. This research was also supported by the World Class University (WCU) program through the National Research Foundation of Korea funded by the Ministry of Education, Science and Technology (Grant no.: R33-10049). The second author is also pleased to acknowledge the support of The Lloyd's Register Educational Trust (The LRET) which is an independent charity working to achieve advances in transportation, science, engineering and technology education, training and research worldwide for the benefit of all.

References

Atluri, S. N. (2002): Methods of Computer Modeling in Engineering and Science. Tech. Science Press, 1400 pages.

Atluri, S. N.; Liu, H. T.; Han, Z. D. (2006): Meshless local Petrov-Galerkin (MLPG) mixed collocation method for elasticity problems. *CMES: Computer Modeling in Engineering & Sciences,* vol. 14, pp. 141-152.

Atluri, S. N.; Shen, S. (2002): The meshless local Petrov-Galerkin (MLPG) method:

a simple & less-costly alternative to finite element and boundary element methods. *CMES: Computer Modeling in Engineering & Sciences,* vol. 3, pp. 11-51.

Cai Y. C.; Paik J. K.; Atluri S. N. (2009): Large Deformation Analyses of Space-Frame Structures, with Members of arbitrary Cross-Section, Using Explicit Tangent Stiffness Matrices, Based on a von Karman Type Nonlinear Theory in Rotated Reference Frames. *CMES: Computer Modeling in Engineering & Sciences,* vol. 53, pp. 117-145.

Cai Y. C.; Paik J. K.; Atluri S. N. (2009): Large Deformation Analyses of Space-Frame Structures, Using Explicit Tangent Stiffness Matrices, Based on the Reissner variational principle and a von Karman Type Nonlinear Theory in Rotated Reference Frames. *CMES: Computer Modeling in Engineering & Sciences,* vol. 54, pp. 335-368.

Cai Y. C.; Paik J. K.; Atluri S. N. (2010): Locking-free Thick-Thin Rod/Beam Element for Large Deformation Analyses of Space-Frame Structures, Based on the Reissner variational Principle and A Von Karman Type Nonlinear Theory. *CMES: Computer Modeling in Engineering & Sciences,* vol. 58, pp. 75-108.

Cai Y. C.; Paik J. K.; Atluri S. N. (2010): A Triangular Plate Element with Drilling Degrees of Freedom, for Large Rotation Analyses of Built-up Plate/Shell Structures, Based on the Reissner Variational Principle and the von Karman Nonlinear Theory in the Co-rotational Reference Frame. *CMES: Computer Modeling in Engineering & Sciences,* vol.61, pp.273-312.

Dai, H. H.; Paik, J. K.; Atluri, S. N. (2011): The Global Nonlinear Galerkin Method for the Analysis of Elastic Large Deflections of Plates under Combined Loads: A Scalar Homotopy Method for the Direct Solution of Nonlinear Algebraic Equations. *CMC: (in print).*

Fan, C. M.; Liu, C. S.; Yeih, W. C.; Chan, H. F. (2010): The Scalar Homotopy Method for Solving Non-Linear Obstacle Problems. *CMC: Computers, Materials & Continua,* vol. 15, pp. 67-86.

Ku, C. Y.; Yeih, W. C.; Liu, C. S. (2010): Solving Non-Linear Algebraic Equations by a Scalar Newton-homotopy Continuation Method. *International Journal of Nonlinear Science & Numerical Simulation,* vol. 11, pp. 435-450.

Liu, C. S. (2000): A Jordan algebra and dynamic system with associator as vector field. *International Journal of Non-Linear Mechanics,* vol. 35, pp. 421-429

Liu, C. S.; Atluri, S. N. (2011a): Simple "Residual-Norm" Based Algorithms, for the Solution of a Large System of Non-Linear Algebraic Equations, which Converge Faster than the Newton's Method. *CMES: Computer Modeling in Engineering & Sciences,* vol.71, pp.279-304.

Liu, C. S.; Atluri, S. N. (2011b): An Iterative Algorithm for Solving a System of Nonlinear Algebraic Equations **F(x)=0**, using the system of ODEs with an optimum α in $\dot{\mathbf{x}} = \lambda \left[\alpha \mathbf{F} + (1-\alpha)\mathbf{B}^{\mathrm{T}}\mathbf{F}\right]$; $B_{ij} = \partial F_i / \partial x$. *CMES: Computer Modeling in Engineering & Sciences, (in print).*

Liu, C. S.; Atluri, S. N. (2009): A Novel Time Integration Method for Solving A Large System of Non-Linear Algebraic Equations. *CMES: Computer Modeling in Engineering & Sciences,* vol. 31, pp. 71-83.

Liu, C. S.; Atluri, S. N. (2008): A Fictitious Time Integration Method (FTIM) for Solving Mixed Complementarity Problems with Applications to Non-Linear Optimization. *CMES: Computer Modeling in Engineering & Sciences,* vol. 34, pp. 155-178.

Liu, C. S.; Atluri, S. N. (2009): A Fictitious Time Integration Method for the Numerical Solution of the Fredholm Integral Equation and for Numerical Differentiation of Noisy Data, and Its Relation to the Filter Theory. *CMES: Computer Modeling in Engineering & Sciences,* vol. 41, pp. 243-261.

Liu, C. S.; Ku, Y. C.; Yeih, W. C.; Fan, C. M.; Atluri, S. N. (2010): An Exponentially Convergent Scalar Homotopy Algorithm for Solving A Determinate/Indeterminate System of Non-Linear Algebraic Equations. *CMES: Computer Modeling in Engineering & Sciences*

Liu, C. S.; Yeih, W. C.; Atluri, S. N. (2010): An Enhanced Fictitious Time Integration Method for Non-Linear Algebraic Equations with Multiple Solutions: Boundary Layer, Boundary Value and Eigenvalue Problems. *CMES: Computer Modeling in Engineering & Sciences,* vol. 59, pp. 301-323.

Liu, C. S.; Yeih, W. C.; Kuo, L. C.; Atluri, S. N. (2009): A Scalar Homotopy Method for Solving an Over/Under-determined System of Non-Linear Algebraic Equations. *CMES: Computer Modeling in Engineering & Sciences,* vol. 53, pp. 47-71.

Paik, J. K.; Thayamballi, A. K.; Lee, S. K.; Kang, S. J. (2001): A semi-analytical method for the elastic–plastic large deflection analysis of welded steel or aluminum plating under combined in-plane and lateral pressure loads. *Thin-Walled Structure,* vol. 39, pp.125–152.

Timoshenko, S.; Krieger, S. W. (1959): Theory of Plates and Shells. McGraw-Hill Companies, 580 pages

Ueda, Y.; Rashed, S. M. H.; Paik, J. K. (1987): An Incremental Galerkin Method for Plates and Stiffened Plates. *Computers & Structures,* vol. 27, pp. 147-156.

Zhu H. H.; Cai Y. C.; Paik J. K.; Atluri S. N. (2010): Locking-free Thick-Thin Rod/Beam Element Based on a von Karman Type Nonlinear Theory in Rotated

Reference Frames For Large Deformation Analyses of Space-Frame Structures. *CMES: Computer Modeling in Engineering & Sciences,* vol. 57, pp. 175-204.

Zhu, T.; Zhang, J.; Atluri, S. N. (1999): A meshless numerical method based on the local boundary integral equation (LBIE) to solve linear and non-linear boundary value problems. *Eng. Anal. Bound. Elem.,* vol. 23, pp. 375-389